

Effects of Buckling on Stress and Strain in Thin Randomly Disordered Tension-Loaded Sheets

Bjørn Skjjetne,^{1,2} Torbjørn Helle,¹ and Alex Hansen²

¹*Department of Chemical Engineering, Norwegian University of Science and Technology, N-7491 Trondheim, Norway*

²*Department of Physics, Norwegian University of Science and Technology, N-7491 Trondheim, Norway*

(Dated: February 8, 2020)

We study how crack buckling affects stress and strain in a thin sheet with random disorder. The sheet is modeled as an elastic lattice of beams where each of the beams have individual thresholds for breaking. A statistical distribution with an exponential tail towards either weak or strong beams is used to generate the thresholds and the magnitude of the disorder can be varied arbitrarily between zero and infinity. Applying a uniaxial force couple along the top and bottom rows of the lattice, fracture proceeds according to where the ratio of the stress field to the local strength is most intense. Since breakdown is initiated from an intact sheet where the first crack appears at random, the onset and mode of buckling varies according to where and how the cracks grow. For a wide range of disorders the stress-strain relationships for buckling sheets are compared with those for non-buckling sheets. The ratio of the buckling to the non-buckling value of the maximum external force the system can tolerate before breaking is found to decrease with increasing disorder, as is the ratio for the corresponding displacement.

PACS numbers: 81.40.Jj, 62.20.-x, 05.40.-a

I. INTRODUCTION

In recent years methods have been developed within the statistical physics community to describe breakdown phenomena in complex media [1]. These are the so-called lattice models, where the material is reduced to a set of points on a grid whereupon disorder is imposed on each of the elements on the grid. The desire to understand structurally non-uniform systems stems from the fact that many materials, natural or man-made, show a significant degree of disorder on the microscopic or mesoscopic level. In order to realistically describe how such materials fracture one has to include the interplay between, on the one hand, local variations in material properties and, on the other hand, a constantly evolving non-uniform stress field. The above mentioned lattice models are especially well suited for this purpose.

Most of the work done with lattice models on fracture and other breakdown phenomena, however, has focused on the fundamental underlying principles rather than traditional problems in fracture mechanics. The various quantities studied have been expressed through scaling laws and critical exponents, often with the aim to shed light on universal aspects of phenomena which are seemingly unrelated. The most common examples besides fracture are transport properties and growth processes [2, 3]. Obviously there is much to benefit from the application of lattice modeling to more specific problems in fracture mechanics, especially where disordered materials are concerned.

By far the most popular tool in fundamental studies of breakdown processes has been the so-called random fuse model [4], a scalar analogue of fracture which really models electrical breakdown. Another model, which

takes account of the vectorial nature of elasticity, is the beam lattice [5, 6]. Recently, we introduced a three dimensional version of the beam lattice which is suitable to describe buckling in thin planar structures [7]. Such buckling behaviour is perhaps most frequently associated with thin plates or beams under compressive loading. In this paper we concern ourselves with the special case of a thin planar structure under tensile, mode-I type, loading. The interaction of buckling with fracture in such cases is a well known phenomenon, although as a problem it remains much less studied.

Most of the data reported, both theoretical and experimental, have centered on a few, rather limited, special cases, such as that of a thin plate with a center-crack, aligned in a perpendicular fashion to the externally applied force. When such a plate is subjected to uniaxial tensile loading, transverse compressive stresses build up in the vicinity of the crack, causing the unsupported edges to deflect out of the initial rest plane. This redistributes the stresses around the crack and leads to a stronger singularity at the tip, thus reducing the external force necessary to propagate crack growth. There are many applications for which the special case of a homogeneous thin plate with a center-crack is representative. Crack buckling, however, is observed under a variety of conditions, and often involves anisotropic or disordered materials with more than one crack.

Composites, for instance, are on the increase as the preferred material for use in the thin walled plate- or shell-structures so essential to the construction of vehicles for transportation purposes, e.g., hulls and fuselages. Critical loads for orthotropic plates have been obtained in finite element (FEM) calculations, but only within the usual single-crack or hole scenario [8]. The importance

of buckling and the way it interacts with fracture in the presence of multiple cracks has been recognized for some time, however. In the aerospace industry, for instance, one seeks to make allowance in the design approach for the presence of multi-site damage, i.e., assess to what extent a series of aligned cracks have on the strength properties of a structure [9, 10]. Moreover, buckling plays an important role in the breaking of thin sheets where the disordered nature of the micro-structure cannot be ignored. The crack geometry which obtains in such cases may be highly complex. A specific example of this is paper. Paper results from a rapid filtration process involving water and wood fibres. The sheet formed is a layered fibre-structure, but nonetheless strongly coupled in the vertical direction. Paper is thus a highly stochastic material, where the essentially random structure is modified by flocculation, i.e., an undesired clustering of fibres in the early stages of the filtration process [11]. With conditions of tensile loading frequently arising in production facilities as well as printing presses, buckling deformations due to tension in paper is a well known phenomenon [12]. Its interaction with fracture has not received sufficient attention, however.

In the following we briefly summarize some of the research that has been done on the buckling of thin sheet materials under tensile loading. Among the earliest investigations was that made by Cherepanov [13] on membranes containing holes. This, and much of the literature which followed mainly concerned itself with the calculation of critical loads for the onset of buckling [14, 15, 16, 17], rather than the effect buckling has on the fracture properties once it has set in, i.e., the so-called post-buckling behaviour. That buckling should adversely affect residual strength has been recognized for some time, however, with early experimental observations reported by Forman [18], Dixon and Strannigan [19], and Zielsdorff and Carlson [20], hence the interest in determining the loads and conditions under which plates with specified parameters buckle. As already noted, the source to this reduction in strength has been traced to a redistribution of stresses which leads to a stronger singularity at the tip of the crack [21, 22, 23].

Most of the results relevant to the critical buckling load have been obtained for thin plates with a center crack. Such results are usually expressed in the form of an empirical relation which involves plate thickness, crack length, Young's modulus and a proportionality factor. In their recent experimental work, Guz and Dyshel have also considered several cases which can be seen as variations on the theme of a central crack; e.g., the effect that crack curvature or an inclination angle has on either the critical buckling load or the residual strength of a plate with a centrally located crack [24]; or the effect a straight central crack has on the critical buckling load of a two-layered plate [25]. Centrally cracked plates are not the only systems studied, however, plates with edge cracks have also been considered. Here the buckling mechanism has been found to be different from that

which causes a central crack to bulge [26]. Critical buckling loads relevant to both perpendicular [27, 28] and inclined [29] edge cracks have been obtained, as well as results for the effect buckling has on the residual strength of edge cracked panels [28].

With regard to modeling and theoretical research, an early study by Pellet et al. employed a Rayleigh-Ritz variational procedure to obtain critical buckling loads in the presence of a circular hole [30]. Recent FEM calculations realistically reproduce the observed buckling behaviour around centrally located cracks, and results have been obtained for critical loads which agree well with experimental findings [15, 17, 21, 22, 23]. The FEM approach has also been used to study the various modes of buckling and the extent of the buckling zone, e.g., for plates with either a perpendicular [21] or an inclined [23] central crack. Gilabert et al. also obtained results relevant to the zone of deformation [31], and critical loads for various crack geometries, e.g., circular holes or rectangular cut-outs with sharp or rounded corners, have been obtained in other FEM calculations [32].

Features of the post-buckling behaviour, other than the shape and extent of the buckling zone, was obtained by Petyt, i.e., for the vibration characteristics of a centrally cracked plate subject to acoustic loads [21]. Petyt also addressed the non-linear nature of FEM calculations for the post-buckling behaviour, and Riks et al. [22] used such an analysis to show that the energy release-rate at the tip of the crack undergoes a sudden increase at the onset of buckling. The stress intensity along the post-buckling path is then larger than that obtained along the pre-buckling path for the same load, a result which, in agreement with experimental observations, indicates that the residual strength of the plate is reduced by buckling. The effect of crack inclination on the energy release-rate in the post-buckling state has also been studied [23]. FEM calculations for the load versus crack-opening length in buckling and non-buckling fracture modes have been carried out in a study by Seshadri and Newman [9], showing a significant reduction in the residual strength. Their work also considered the effect of plasticity by assuming a hypothetical material with a very high crack-tip opening angle, with the reduction in strength due to buckling now being generally less pronounced than in the brittle case.

As the above summary shows, practically all previous work considers the effect buckling has on the strength properties of an already cracked plate, or a plate with a geometrical discontinuity such as a circular hole or a rectangular cut-out. In other words, if the physical parameters of the plate are such that buckling can be expected before the crack begins to grow, the residual strength of the plate will be significantly lower than what would otherwise be expected, based on an analysis which does not take account of buckling. The present study of fracture and buckling is fundamentally different in the sense that we regard a sheet which, in its initial state, has no cracks or other discontinuities. Instead, cracks form by a com-

plex process which depends on the evolving distribution of stresses and its interaction with a disordered meso-structure. The onset of buckling in this scenario, and the effect buckling has on the fracture properties, will vary according to the type of disorder used, i.e., weak or strong. Whereas for strong disorders there will be significant sample-to-sample variations, such variations tend to be less pronounced for weak disorders. However, even for weak disorders the final crack which breaks the system will only rarely appear at the exact center of the sheet, and even then the situation might be complicated by additional cracks in the vicinity – cracks which interact with the main crack so as to alter the distribution of stresses and hence also the exact shape or mode of buckling. Therefore, due to the statistical nature of the results obtained, features such as the extent of the buckling zone, or the shape of the deflected crack edge, will not at present be dealt with in any detail. For the same reasons critical loads are not calculated, since the magnitude of this quantity depends on very specific sheet parameters, i.e., for a given sheet thickness the critical load has been shown to depend on the ratio of the crack length to the sheet width.

II. THE BEAM LATTICE

The beam lattice used in our calculations is a regular square lattice, where each beam has unit length. System size L therefore corresponds to the number of beams along the top or bottom rows. The nodes are equidistantly spaced along $J = L + 2$ horizontal rows and $I = L + 1$ vertical columns, each having four nearest neighbours to which it is fastened by elastic beams. When nodes are displaced the angle at the joint where two beams come together remains perpendicular, thus inducing shearing forces and bending moments in addition to axial tension or compression.

In the plane beam lattice there are three degrees of freedom for the displacement of nodes, i.e., translation along either the X -axis or the Y -axis, and rotations about the Z -axis. The displacement field is obtained by requiring the sum of forces and moments on each node to be zero. Specifically, we solve

$$\sum_j D_{ij} \begin{bmatrix} x_i \\ y_i \\ w_i \end{bmatrix} = \lambda \begin{bmatrix} X_i \\ Y_i \\ W_i \end{bmatrix}, \quad (1)$$

where the forces on node i are

$$X_i = {}_x A_i^{(1)} + {}_x T_i^{(2)} + {}_x A_i^{(3)} + {}_x T_i^{(4)}, \quad (2)$$

$$Y_i = {}_y T_i^{(1)} + {}_y A_i^{(2)} + {}_y T_i^{(3)} + {}_y A_i^{(4)}, \quad (3)$$

$$W_i = \sum_{j=1}^4 {}_w M_i^{(j)}, \quad (4)$$

by numerical relaxation, i.e., the conjugate gradient method [33], to obtain the set of displacements which minimizes the elastic energy of the lattice.

In Eqs (2) and (3), A and T denote axial and transverse force, respectively, while in Eq. (4) M denotes the bending moment. Hence, ${}_x A_i^{(3)}$ is the force exerted on node i from $j = 3$ along the X -axis by axial tension or compression. Neighbouring nodes are numbered anti-clockwise, starting with $j = 1$ on the left.

Defining $\delta r = r_j - r_i$, where $r \in \{x, y, w\}$, the contributions from $j = 1$ are

$${}_x A_i^{(1)} = \frac{1}{\alpha} \delta x, \quad (5)$$

$${}_y T_i^{(1)} = \frac{1}{\beta + \frac{\gamma}{12}} \left[\delta y - \frac{1}{2} (w_i + w_j) \right], \quad (6)$$

$${}_w M_i^{(1)} = \frac{1}{\beta + \frac{\gamma}{12}} \left[\frac{\beta}{\gamma} \delta w + \frac{\delta y}{2} - \frac{1}{3} (w_i + \frac{w_j}{2}) \right], \quad (7)$$

where

$$\alpha = \frac{1}{E\rho}, \quad \beta = \frac{1}{G\rho}, \quad \gamma = \frac{1}{EI}, \quad (8)$$

are the prefactors characteristic of the material and its dimensions, i.e., E is Young's modulus, ρ and I the area of the beam section and its moment of inertia, respectively, and G the shear modulus [6].

The fracture process consists of removing one beam at a time, whereby a new set of displacements are obtained at each step by solving Eq. (1). The criterion by which a beam is removed from the lattice depends on the ratio of the local stress to the breaking threshold. Using t_A and t_M for the maximum thresholds in axial force and bending moment, respectively, a good breaking criterion [6] inspired from Tresca's theory is

$$\left(\frac{A}{t_A} \right)^2 + \frac{|M|}{t_M} \geq 1, \quad (9)$$

where $|M| = \max(|M_i^{(j)}|, |M_j^{(i)}|)$ is the largest of the moments at the two beam ends i and j .

The time taken for mechanical equilibrium to be reached is assumed to be much shorter than the time taken to remove a beam, i.e., the fracture process is assumed to be quasi-static. It is driven by imposing a fixed unit displacement on the top row of the lattice. Since internal displacements, forces and moments are proportional to this, the actual external elongation of the lattice is obtained by determining the minimum value of the proportionality constant λ_L in

$$\left(\lambda_L \frac{A}{t_A} \right)^2 + \lambda_L \frac{|M|}{t_M} = 1, \quad (10)$$

from which the external force is obtained as

$$f_L = \lambda_L \sum_{i=1}^{I(J-1)} {}_y A_i^{(2)} n_{i,y}, \quad (11)$$

with the array

$$n_{i,y} = \begin{cases} 1, \\ 0, \end{cases} \quad (12)$$

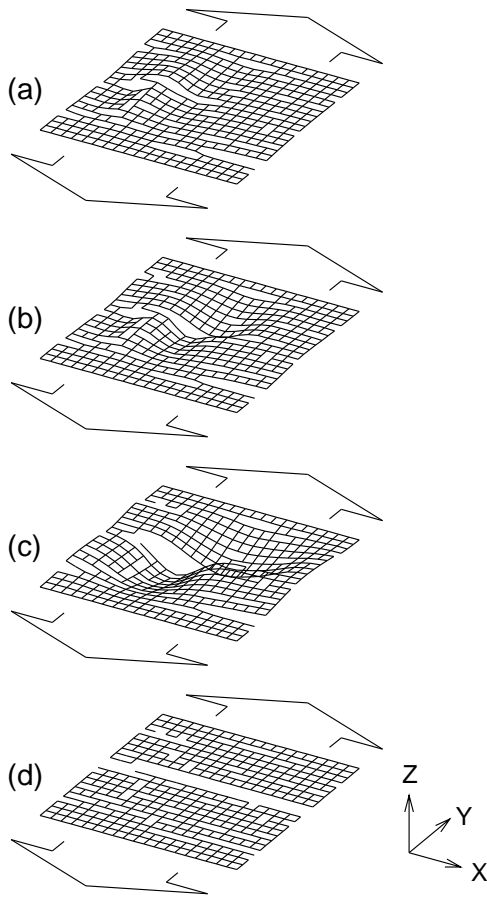


FIG. 1: A disordered lattice of size $L = 20$, shown at four different stages in the breakdown process. The lattice is strained to failure by applying a force couple at the top and bottom. With the appearance of large cracks, the structure is seen to deflect out of the initial rest plane. The number of broken beams in this simulation are, from (a) to (d), $N = 65, 72, 78,$ and 86 , respectively.

keeping track of whether beams are intact (1) or have been broken (0), respectively.

In Eq. (11), contributions other than ${}_y A_i^{(2)}$ cancel when the sum is over the entire lattice. This is due to the square lattice topology and the nature of the external boundary conditions applied, i.e., mode-I type loading in the Y -direction. Regarding the internal forces, the same term continues to be the sole non-zero contribution when the lattice is intact. Consequently the first beam to break is that for which the ratio A/t_A is the largest. After this has been removed, however, bending moments M and

transverse forces T (including shear) are induced in the immediate neighbourhood of the beam. This is due to the screening effect of the “hole”, or crack, created by its removal from the lattice.

A thin sheet will usually display deviations in symmetry with respect to the thickness, e.g., there may be variations in the thickness itself or there may be a gradient in the structural properties of the material. An example of the latter is paper, where, due to the process by which it is manufactured, the fibre structure on one side always has a stronger orientational bias. In other materials the density varies in the thickness direction. When a uniaxial force couple is applied on opposite edges of the sheet, such variations create bending moments about axes in parallel within the XY -plane, see Fig. 1, which shows the coordinate system and the direction of the external load. In fact, when the internal stresses (which arise as a consequence of the external load condition) combine with certain crack configurations, minute deviations of the symmetry plane itself from a perfect two dimensional embedding will be sufficient to cause buckling. Numerous studies have been reported in the literature concerning the external load necessary to cause buckling, e.g., for a sheet with a central crack the magnitude of the critical load has been found to decrease with decreasing sheet thickness and increasing crack extent.

The additional terms which cause buckling are much smaller in magnitude than those governing the forces within the plane lattice. There is, however, a non-separable relationship between in-plane and out-of-plane displacements which causes the in-plane coordinates of the non-buckling lattice to change significantly when buckling is allowed. For this reason the X_i, Y_i and W_i components of the buckling lattice [7]

$$\sum_j D_{ij} \begin{bmatrix} u_i \\ v_i \\ w_i \\ x_i \\ y_i \\ z_i \end{bmatrix} = \lambda \begin{bmatrix} U_i \\ V_i \\ W_i \\ X_i \\ Y_i \\ Z_i \end{bmatrix} \quad (13)$$

contain additional non-linear terms, i.e., terms not included in Eq. (1).

Specifically, the axial force component

$$X_i^{(1)} = \frac{1}{\alpha} \delta x \quad (14)$$

in Eq. (1) is replaced by

$$X_i^{(1)} = -F_i^{(1)} \left[\cos w_i \cos u_i - \frac{\delta w}{2} \cos \delta w \sin w_i - \frac{\delta u}{2} \cos \delta u \sin u_i \right] \\ + \frac{1}{\beta + \frac{\gamma Z}{12}} \left[(1 + \delta x) \sin w_i - \delta y \cos w_i + \frac{\delta w}{2} \right] \sin w_i + \frac{1}{\beta + \frac{\gamma Y}{12}} \left[(1 + \delta x) \sin u_i - \delta z \cos u_i + \frac{\delta u}{2} \right] \sin u_i, \quad (15)$$

where

$$F_i^{(1)} = \frac{1}{\alpha} \left\{ 1 - \frac{\delta u}{2} \left[\sin\left(\frac{\delta u}{2}\right) \right]^{-1} \sqrt{\delta z^2 + (1 + \delta x)^2} \right\} \quad (16)$$

is the force along the axis of the beam, including an angular correction which takes into account the additional elongation due to bending. Likewise, the transverse force

$$Y_i^{(1)} = \frac{1}{\beta + \frac{\gamma}{12}} \left[\delta y - \frac{1}{2}(w_i + w_j) \right] \quad (17)$$

is replaced by

$$Y_i^{(1)} = -F_i^{(1)} \left(\sin w_i \cos u_i - \frac{\delta w}{2} \cos \delta w \cos w_i \right) - \frac{1}{\beta + \frac{\gamma Z}{12}} \left[(1 + \delta x) \sin w_i - \delta y \cos w_i + \frac{\delta w}{2} \right] \cos w_i, \quad (18)$$

and the in-plane moment

$$W_i^{(1)} = \frac{1}{\beta + \frac{\gamma}{12}} \left[\frac{\beta}{\gamma} \delta w + \frac{\delta y}{2} - \frac{1}{3} \left(w_i + \frac{w_j}{2} \right) \right] \quad (19)$$

is replaced by

$$W_i^{(1)} = \frac{\beta}{\gamma Z (\beta + \frac{\gamma Z}{12})} \delta w - \frac{1}{2(\beta + \frac{\gamma Z}{12})} \left[(1 + \delta x) \sin w_i - \delta y \cos w_i + \frac{\delta w}{3} \right] - F_i^{(1)} \frac{\delta w}{4} \cos \delta w. \quad (20)$$

The additional terms of Eq. (13) are

$$Z_i^{(1)} = -F_i^{(1)} \left(\sin u_i + \frac{\delta u}{2} \cos \delta u \cos u_i \right) - \frac{1}{\beta + \frac{\gamma Y}{12}} \left[(1 + \delta x) \sin u_i - \delta z \cos u_i + \frac{\delta u}{2} \right] \cos u_i \quad (21)$$

for the displacements normal to the XY -plane, and

$$U_i^{(1)} = \frac{\beta}{\gamma Y (\beta + \frac{\gamma Y}{12})} \delta u - \frac{1}{2(\beta + \frac{\gamma Y}{12})} \left[(1 + \delta x) \sin u_i - \delta z \cos u_i + \frac{\delta u}{3} \right] - F_i^{(1)} \frac{\delta u}{4} \cos \delta u \quad (22)$$

for the rotations about the Y -axis. Finally,

$$V_i^{(1)} = \xi \delta v \quad (23)$$

is the torque of the beam when rotations are about the X -axis. Assuming $w > t$,

$$\xi = G \frac{wt^3}{3} \quad (24)$$

is the torsional moment of inertia in Eq. (23), with w denoting the width of the beam cross section and t its thickness. Assuming a rectangular cross-section, the moments of inertia for bending are

$$I_Z = \frac{1}{12} w^3 t \quad (25)$$

within the XY -plane, and

$$I_X = \frac{1}{12} wt^3 = I_Y \quad (26)$$

within the YZ - and XZ -planes, respectively.

The expressions for the forces acting on the beams in Eqs. (15) to (23) have been derived by considering an

elastic beam with no end restraints [34], where the ratio of the beam width to the thickness presently has been set to 10:1. With regard to bending flexibility, the lattice is now more pliable in the out-of-plane direction, as would be expected for a thin sheet material.

In lattice modeling the rule by which a beam is broken can be specified according to the properties of the material one wishes to study. Presently the fracture criterion is taken to depend on a combination of axial stress, bending and torsion. Hence, we assume

$$\left(\frac{F_C}{t F_C} \right)^2 + \frac{|\mu_C|}{t_{\mu_C}} \geq 1, \quad (27)$$

where

$$F_C = F_i^{(j)} - \chi |Q_i^{(j)}| \quad (28)$$

is the effective stress, and

$$Q_i^{(j)} = \sum_{k=1,3} \delta_{kj} V_i^{(j)} + \sum_{k=2,4} \delta_{kj} U_i^{(j)} \quad (29)$$

is the torque. Moreover, with μ_C denoting the combined bending moment and

$$\sigma = \frac{w}{t} \quad (30)$$

being the aspect ratio of the cross section of the beam, the expression

$$\chi = \begin{cases} 1 + (\sigma L)^2 |F_i^{(j)}|, & F_i^{(j)} < 0, \\ 1, & F_i^{(j)} \geq 0, \end{cases} \quad (31)$$

is an enhancement factor in Eq. (28). In Eq. (29) the Kronecker delta has been used to distinguish between the four neighbouring beams.

Angular displacements about the X - or Y -axis in Eq. (27) activate the stress enhancement mechanism. This increases the stress in a beam when it is under axial tensile loading. Specifically, the larger the the load is, the more sensitive the beam will be to the presence of a certain amount of axial torque. Compressive loads are assumed to be less important, with torque now instead removing some of the axial compression.

The exact mechanism by which buckling alters the rupture mode of a thin sheet will probably vary according to material properties, structural composition, and so on. In many cases it is a well known fact that the work required to drive a crack across a given area is much smaller in mode-III tearing than in pure mode-I tension, as is easily verified with a piece of paper. Transverse forces, however, are not presently assumed to contribute. This is because the disorder of the sheet is modeled on a mesoscopic scale. In a material such as paper, tearing is a shear displacement which affects material properties on much smaller scales, e.g., on the level of the individual fibres. In the beam lattice, on the other hand, each individual beam is representative of the sheet on the level of fibre flocculations. The effect of mode-III crack propagation is instead included by the above combination of torsion and axial stress.

III. NUMERICAL SCHEME OF CALCULATIONS

Mathematically, conjugate gradients is an iterative method to obtain the minimum of a quadratic expression, in our case the elastic energy. For the energy to be quadratic, however, the forces involved must be linear. In obtaining a numerical solution, therefore, the presence of non-linear terms is a complicating factor. Nonetheless, provided the proper numerical safeguards are employed, the correct minimum can be found effectively by use of conjugate gradients. Specifically,

$$\sum_{j=1}^4 X_i^{(j)} = \sum_{j=1}^4 Y_i^{(j)} = \sum_{j=1}^4 W_i^{(j)} = 0 \quad (32)$$

is the solution obtained by relaxing the in-plane coordinates while keeping the out-of-plane coordinates fixed.

Since the leading terms of X_i , Y_i and W_i are all linear, the actual solution for this in-plane projection always lies close to its linear solution. It is found by re-initializing the search, each time using conjugate gradients starting from the previous linear approximation. This is repeated until the minimum stops changing, typically 6-7 searches are required, with convergence being rapid.

After this intermediate solution has been obtained, it is frozen, whereupon the out-of-plane coordinates are relaxed, one at a time. In this case, however, the leading terms are non-linear. Consequently a single search is made toward the minimum to obtain

$$\sum_{j=1}^4 Z_i^{(j)} \approx 0, \quad (33)$$

i.e., a partial only, or (at best) very approximate, solution. Moreover, in order to ensure that this incomplete move carries towards (and not away from) the minimum, the step size of the conjugate gradient iterations in this phase is reduced to a much smaller value.

Likewise, the out-of-plane angular displacements are updated, one at a time, using the same down-scaled step size, to obtain

$$\sum_{j=1}^4 U_i^{(j)} \approx 0, \quad \sum_{j=1}^4 V_i^{(j)} \approx 0, \quad (34)$$

while keeping all other coordinates fixed.

After re-setting the iterational step size, the whole procedure outlined above is repeated. The updated coordinates obtained for the out-of-plane displacements, approximate as they are, do nonetheless cause the in-plane displacements to change. As the final buckled configuration of the lattice is approached the quality of the intermediate partial solutions, represented by Eqs. (33) and (34), gradually improves.

Hence, after a number of repetitions we obtain

$$\sum_{j=1}^4 X_i^{(j)} = \sum_{j=1}^4 Y_i^{(j)} = \dots = \sum_{j=1}^4 V_i^{(j)} = 0, \quad (35)$$

for the sum of forces and moments on all nodes. The previous set of displacements is now identical to the current set of displacements, the calculation having converged upon the final solution.

IV. DISORDER

Each time a beam is broken, a new set of displacements is calculated according to the scheme outlined in section III. A fundamental factor deciding how the lattice breaks is the choice made for the type and magnitude of disorder in the distribution of breaking thresholds. One of the reasons why lattice models are practical is the ease with which such disorder may be included.

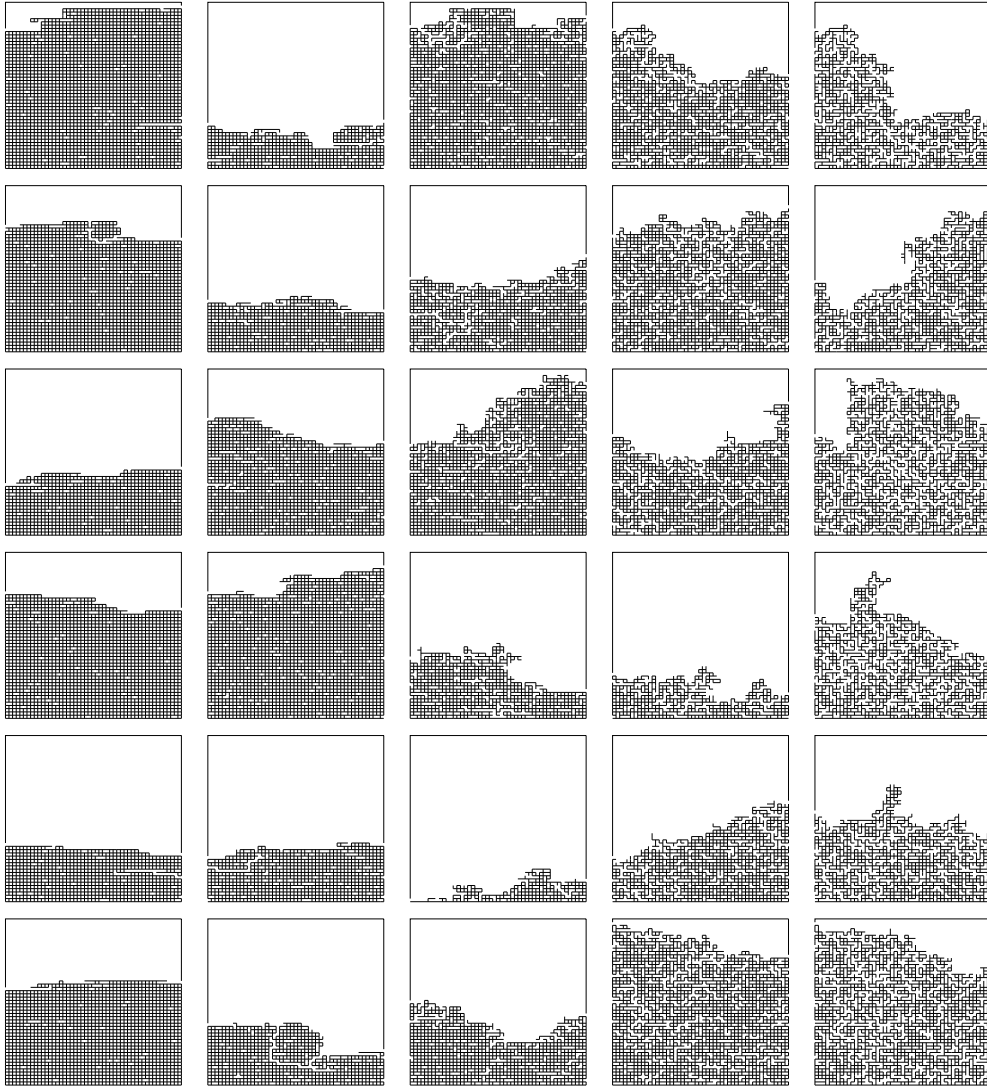


FIG. 2: The lower remaining part of a beam lattice of size $L = 50$ after it has been broken completely, shown for five different disorders, i.e., from left to right: $D = 0.25$, $D = 0.5$, $D = 1$, $D = 2$ and $D = 4$, respectively. From top to bottom, six different samples have been included in each case, the only difference between the samples being the random casts generated for the breaking thresholds.

Presently we generate a random number r on the unit interval $[0, 1]$ and let this represent the cumulative threshold distribution. In Eq. (27) the breaking thresholds are now assigned as $t = r^D$, with

$$p(t) = \frac{1}{D} t^{\frac{1}{D}-1} \quad (36)$$

being the probability density. The same distribution is assumed for the threshold in axial force, $t = t_{FC}$, and bending moment, $t = t_{\mu C}$, with the random casts, however, being different in the two cases.

There are now two types of distribution, i.e., $D > 0$, in which case

$$P(t) = t^{\frac{1}{D}} \quad (37)$$

is a cumulative distribution with bounds $0 \leq t < 1$, and $D < 0$, in which case

$$P(t) = 1 - t^{\frac{1}{D}} \quad (38)$$

is a cumulative distribution with bounds $1 \leq t < \infty$. In this prescription $D = 0$ corresponds to no disorder. As $|D|$ increases the coefficient of variation with respect to any two random numbers r and r' on the interval $[0, 1]$ also increases, with the coefficients for $D > 0$ and $D < 0$ being reciprocal but otherwise the same. Hence, large values of $|D|$ correspond to strong disorders and small values to weak disorder. A few examples for $D > 0$ have been included in Fig. 2, where the bottom part of the broken lattice is shown for five different disorders. Also shown is the sample-to-sample variation for each of the

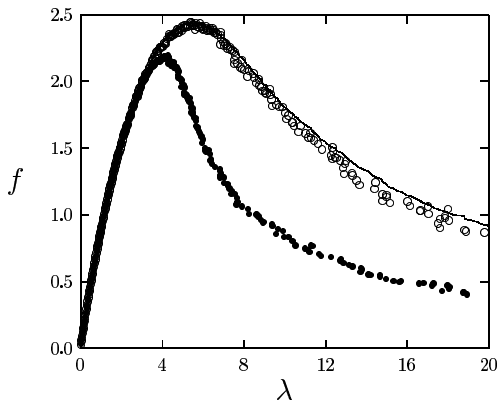


FIG. 3: Force f versus displacement λ for an $L = 32$ lattice with disorder $D = 1$. The two upper curves denote non-buckling fracture, with the continuous line representing Eq. (1) and open circles representing Eq. (13) with buckling suppressed. The lower curve (filled circles) denotes buckling fracture, i.e., the results of Eq. (13) with the out-of-plane degrees of freedom now included.

disorders. For a given magnitude of D , the position of the final crack which breaks the system is seen to vary from one sample to the next, as is its morphology. As the disorder increases, so does the roughness of the crack interface. The number of beams removed also increases with the disorder, i.e., the $D = 4$ samples are seen to be somewhat more diluted than the $D = 2$ samples. In Eq. (36), $D > 0$ and $D < 0$ represent widely different types of distribution. While the former is a power law with a maximum threshold of one, and a tail which extends toward zero, the latter is a power law bounded below by a minimum threshold of one, but now with a tail which extends toward infinity. Both $D > 0$ and $D < 0$ are included in the present calculations.

In the past many different distributions have been used to generate random breaking thresholds. However, as shown by Hansen et al. [35], as the system size diverges only the power law tails of the distribution, if they exist, towards zero or infinity should matter. Hence the use of D as a parameter is very convenient, enabling the asymptotic behaviour of the fracture process to be fully explored as a function of the disorder.

V. STRESS AND STRAIN

In the absence of structural disorder the crack now grows laterally from the site of the first beam removed, taking the shortest possible path across the lattice. Since in our model the beams are linearly elastic up to the breaking threshold, the first break triggers catastrophic rupture. Stress and strain evolves differently in the presence of disorder. Now there are two competing mechanisms for crack growth. On the one hand, the presence of a crack causes stress to be intensified in its immediate vicinity, thereby lending bias towards the growth of al-

ready existing cracks. On the other hand, variations in material strength dictate that new cracks should instead appear in regions which are structurally weak. Which of the two mechanisms is the most important depends on the disorder regime. While in the case of strong disorder fracture is initially disorder dominated, it tends to be localized from the very beginning in the case of weak disorder. For strong disorders small cracks appear at random in the early stages of the process. Here the dominating feature is a wide distribution of breaking thresholds. Since the weakest beams tend to be removed first, the distribution gradually narrows as more beams are removed. Simultaneously, with a growing number of cracks appearing on the lattice, a highly non-uniform stress field develops. In other words, the distribution of stresses widens. At the point where the fracture process goes from being disorder dominated to stress dominated, crack growth becomes localized [35]. Smaller cracks now merge into a single dominating crack and the evolution of stress with strain goes from being stable to unstable.

For a system of size $L = 32$ and disorder $D = 1$, a comparison between the buckling and non-buckling stress-strain characteristics is shown in Fig. 3. The average stress and the average strain has been computed for every beam broken, and the number of samples involved is 10000 in the non-buckling case and 975 in the buckling case. Also included is the result of Eq. (13) with the out-of-plane degrees of freedom suppressed. This result is based on 525 numerical realizations. The agreement between the non-buckling results of Eqs. (1) and (13) is seen to be excellent, especially in the controlled and early catastrophic regimes. Towards the end of the catastrophic regime the loads obtained with Eq. (13) are very slightly lower than those that are obtained with Eq. (1), a result which can be ascribed to the presence of non-linear terms in the former. With buckling, a significant reduction is obtained in both maximum strength and displacement. There is also a notable difference in the shape of the curve within the catastrophic regime. Here

TABLE I: Ratio of buckling to non-buckling maxima, obtained for the external displacement λ and force f , for disorder $D = 1$. The total number of samples calculated is S , and L is the system size.

L	λ_Z/λ_0^a	f_Z/f_0	S_Z	S_0
14	0.83	0.93	1500	5000
17	0.92	0.94	500	2500
20	0.79	0.92	1000	1000
23	0.83	0.92	203	800
27	0.83	0.91	328	600
32	0.75	0.90	975	10000
40	0.74	0.89	210	1400
50	0.77	0.91	70	1750
63	0.77	0.89	110	700
80	0.80	0.92	55	550

^aQuantities labeled Z refer to the buckling case.

the response is less stable with respect to displacement control. That is, the force in the catastrophic regime falls off more rapidly as the displacement increases.

Stress and strain for a range of system sizes is shown in Fig. 4 for the same disorder, i.e., $D = 1$. In calculations for the non-buckling beam lattice, involving a much larger range of sizes [36], the scaling with L of the top of the stress-strain curve is found to be characterized by an exponent close to unity. The stress-strain curves can then be made to collapse onto each other by scaling the axes according to

$$f/L^\gamma = \phi(\lambda/L^\gamma), \quad (39)$$

where $\gamma \approx 1$ and ϕ is a scaling function. Since there is no reason why the buckling system should behave according to different laws in this respect, the reduction in stress and strain should itself be proportional to system size. As was noted in section II, fracture is initiated by imposing on the top row of the lattice a displacement of one beam length. Hence, to avoid scale effects on the buckling behaviour, one of the factors L introduced in the stress enhancement factor, i.e., in Eq. (31), is a scale factor. Without this factor, a different value of the exponent γ would be obtained in Eq. (39). With the current choice of parameters, maximum stress and strain in the buckling and non-buckling cases scale according to the same law, as can be seen from Fig. 4, and

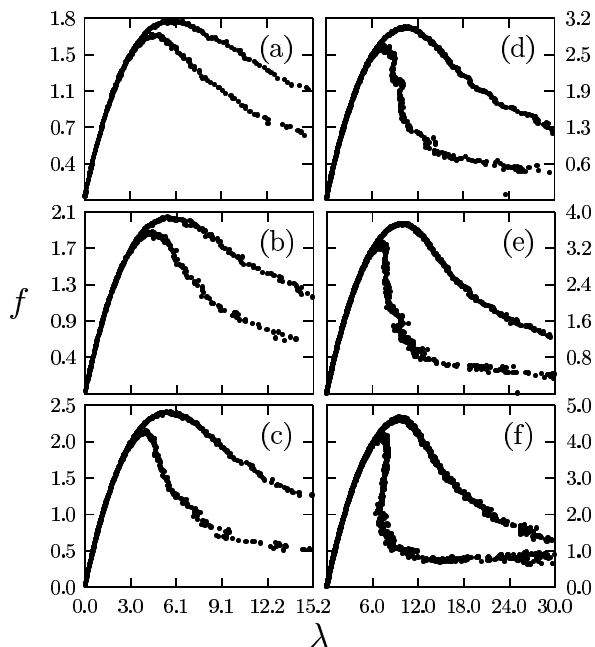


FIG. 4: Force f versus displacement λ for a range of system sizes with disorder $D = 1$, i.e., for (a) $L = 23$, (b) $L = 27$, (c) $L = 32$, (d) $L = 40$, (e) $L = 50$ and (f) $L = 63$. In each case the top curve is the non-buckling result of the simple beam model, calculated from Eq. (1), and the curve below is the buckling result, calculated from Eq. (13). The labels on the axes are scaled down from those in plot (f), being otherwise proportional to system size.

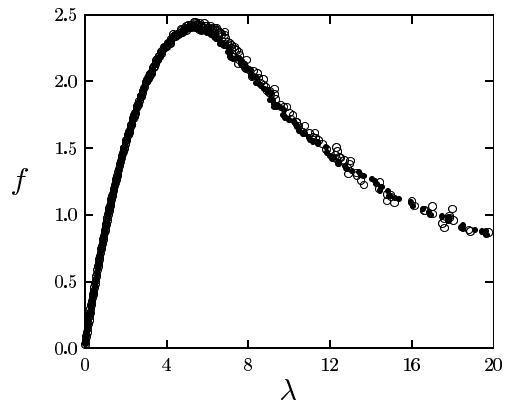


FIG. 5: Force f versus displacement λ for an $L = 32$ lattice with disorder $D = 1$, comparing the buckling (filled circles) and the non-buckling (open circles) results of Eq. (13) where, in the former case, $\chi = 0$ in Eq. (28).

also from the comparison of buckling and non-buckling stress-strain maxima in Table I. Here the values obtained for the reduction in maximum stress and strain appear to be consistent for systems larger than about $L = 20$. Below this, finite size effects become apparent. The most reliable estimates are obtained with the largest number of calculated samples, hence, for $D = 1$, buckling reduces the maximum strength by about 10% and the maximum displacement by about 25%. The shape of the curve in the catastrophic regime varies according to system size. Beyond the turn-over point between stable and unstable crack growth, rupture in the non-buckling system is seen to become increasingly less stable as the size of the system increases. This effect is even more pronounced when the sheet is allowed to buckle.

Significant differences are evident in a comparison between the force or displacement fields of, say, a uniform center-cracked lattice in the case of buckling with the corresponding force or displacement fields in the non-buckling case. Specifically, the transverse forces near to the crack edges, which are compressive in the non-buckling lattice, are released when the lattice buckles, causing the flanks of the crack to deflect. Since the alterations in the force or displacement fields extend beyond the immediate neighbourhood of the crack tips, one may ask whether these effects in themselves are sufficient to bring about a reduction in the maximum load carrying capacity of the lattice. The mechanism by which the stress is intensified at the crack tips, however, takes place on a scale smaller than the individual beam, which is why the fracture criterion Eq. (27) has been augmented by the factor χ . Hence, the hypothetical case of fracture where buckling does not induce intensified stress at the crack tips can be investigated simply by setting $\chi = 0$ in Eq. (28). In Fig. 5 the result is compared with that obtained in non-buckling fracture. Clearly, the evolution of stress with strain is seen to be the same in both the stable and catastrophic regimes. Both curves were obtained from Eq. (13), based on 1350 samples in the buckling case

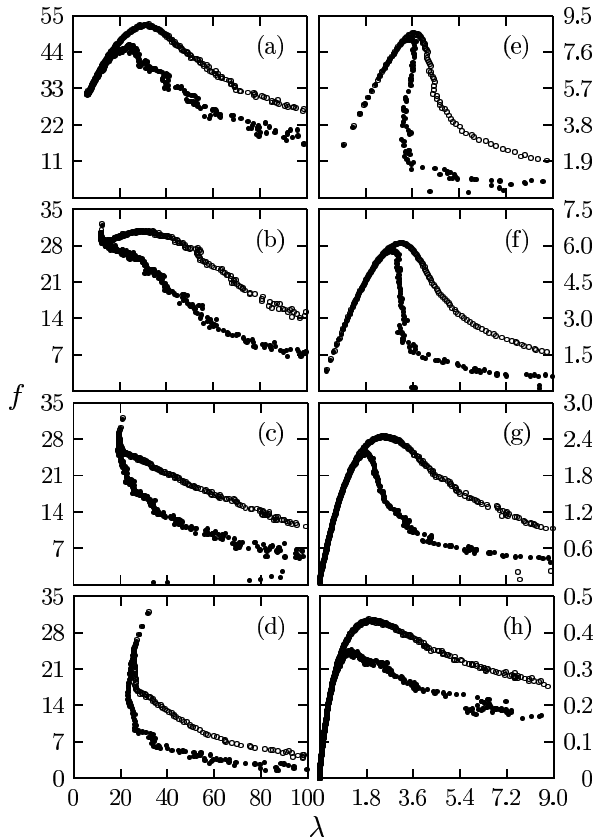


FIG. 6: Force f versus displacement λ obtained for a lattice system of size $L = 32$, for a range of disorders with both $D < 0$ and $D > 0$. On the left are shown (a) $D = -5$, (b) $D = -3$, (c) $D = -2$ and (d) $D = -1$. On the right are shown (e) $D = 0.33$, (f) $D = 0.5$, (g) $D = 1$ and (h) $D = 2$. In (a)–(c) the respective scales on λ are $\times 5$, $\times 2.5$ and $\times 1.5$ that in (d), and in (e)–(g) the respective ratios f/λ are 0.38, 0.3, and 0.15. In all cases the stress-strain curve for buckling lies below that which does not buckle.

and 525 samples in the non-buckling case. One can thus state with certainty that it is the intensified stress at the crack tips, due to a coupling between in-plane and out-of-plane deformations, rather than the re-distribution of stresses within the buckling zone (but away from the immediate neighbourhood of the crack tips) which causes the reduction in residual strength.

In Fig 6 is shown the effect disorder has on the interaction of buckling with fracture. Plots on the left-hand side display stress-strain curves for $D < 0$ type disorder. Here the initial response, i.e., the linear relationship which extends from the origin to the data point of the first broken beam, has been omitted. There is no tail towards zero in the distribution of thresholds here, and consequently there are no broken beams on this part of the curve. In plot (d), where $D = -1$, the first beam to break triggers a catastrophic rupture mode which backtracks along the initial linear response for the first few breaks. It then encounters a vertical section of the curve where several values of f correspond to the same λ . If

TABLE II: Ratio of buckling to non-buckling maxima, obtained for the displacement λ and force f , for $L = 32$. The number of samples is S , and D is the disorder.

D	λ_Z/λ_0^a	f_Z/f_0	S_Z	S_0
0.2	1.	1.	200	500
0.333	0.98	0.97	200	500
0.5	0.92	0.96	280	3500
1	0.75	0.90	975	10000
2	0.65	0.81	192	1000

^aQuantities labeled Z refer to the buckling case.

displacement control is applied and relaxed sufficiently fast for the crack to be halted at this point, we have a situation of conditional stability where a slight perturbation, say a bump or a jar, suffices to further propagate the crack (this refers to the average situation, with individual samples being subject to fluctuations). Otherwise, applying displacement control without this sudden relaxation, the crack develops catastrophically until it is arrested when encountering strong beams in the tail towards infinity. From here on, the force continues to fall off as the displacement is increased.

The main effect buckling has for weak $D < 0$ disorder is to make the force fall off more rapidly in the catastrophic regime. Additionally, the section of the curve which is conditionally stable in the non-buckling case is rendered unstable, i.e., the curve turns back on itself. As $|D|$ increases there is a turn-over in the average stress-strain behaviour in the sense that, beyond $D = -3$, force control may be applied without necessarily triggering catastrophic rupture. This, of course, is due to the presence of a large number of beams with high breaking thresholds. When the tail towards infinity becomes sufficiently strong, in other words, the number of beams which can be found in the vicinity of the lower bound becomes a minority. The stress-strain relationship then attains a similar form to that of $D > 0$, except now fracture starts at a finite displacement or force. Although in (a) the controlled regime, which obtains after the first beam breaks, contains a smaller number of broken beams than does, for instance, the one in (g), the reduction in force and displacement due to buckling is comparable in the two cases. The reason for this is a more intense stress field in the former case, caused by higher thresholds, which in turn moves the onset of buckling to an earlier stage of the fracture process.

Displayed on the right-hand side are stress-strain curves with $D > 0$ type disorder. These are mostly subject to the same features as the result of Fig. 3, relevant to $D = 1$. An exception, perhaps, is $D = 2$, for which the stability in the catastrophic regime appears to be unchanged by buckling. For $D = 2$ and beyond, however, the number of beams relevant to the catastrophic regime is small compared to that of the controlled regime. This means that the number of samples which contribute decreases toward the end of the stress-strain curve (the

curves have not been truncated at the average number of broken beams), and hence statistical fluctuations become large in this region.

Whereas for weak $D > 0$ disorders only a small reduction is obtained in the maximum of stress and strain, the stability in the catastrophic regime of fracture is significantly affected in this case, as can be seen from (e) in Fig. 6, i.e., for $D = 0.33$. The reason is the onset of buckling, which for low disorders occurs near the top of the curve. Even when the disorder is sufficiently low for the onset of buckling, in average, to occur after the top has been reached, a slight decrease in maximum strength may be expected. This, of course, is due to the fact that a number of samples will buckle prior to this average onset.

In Table II, results for the $L = 32$ system are shown for a range of disorders with $D > 0$. Here the decrease in force and displacement is seen to depend on the magnitude of D , i.e., as $|D|$ increases buckling has an increasingly adverse effect on both the maximum load and the maximum displacement a disordered system can sustain. The maximum displacement is more strongly affected than the maximum load.

VI. SUMMARY

The breaking characteristics of thin sheets with structural disorder have been obtained in numerical simulations which include the out-of-plane buckling behaviour.

The model used is an elastic lattice of beams where each beam is representative of the scale of the structural disorder. Depending on the magnitude of disorder, breakdown is either localized to the first point of damage or initially a random cracking process which at a later stage crosses over to localized fracture behaviour.

The breakdown process is initiated from an initially intact sheet, where buckling sets in after a certain amount of damage has occurred. Specifically, the onset of buckling varies considerably according to both the size and configuration of the emerging cracks. Given a certain system size and disorder, several numerical realizations of a sheet are generated, corresponding to different sets of random breaking thresholds. The statistical properties are then obtained from the average behaviour based on the disorders and sizes chosen.

As in the case of uniform pre-cracked sheets, it is found that buckling adversely affects the external force and displacement a randomly disordered sheet can sustain in mode-I type tensile loading. The degree to which the maximum force and displacement is reduced depends on the magnitude of the disorder. For instance, in a material such as paper this would mean that buckling should affect the maximum load carrying capacity more adversely in the case of a fibre-web with uneven formation than one with a more even formation. When the meso-scale disorder is low the reduction in strength is insignificant and it is the catastrophic regime which is most affected, now being less stable.

-
- [1] See, e.g., H. J. Herrmann and S. Roux, *Statistical Models for the Fracture of Disordered Media*, (North-Holland, Amsterdam, 1990).
- [2] A. L. Barabasi and H. E. Stanley, *Fractal Concept in Surface Growth*, (Cambridge University Press, Cambridge, England, 1995).
- [3] E. Bouchaud, *J. Phys. Condens. Matter* **9**, 4319 (1997).
- [4] L. de Arcangelis, S. Redner and H. J. Herrmann, *J. Phys. (Paris) Lett.* **46**, L585 (1985).
- [5] S. Roux and E. Guyon, *J. Phys. (Paris) Lett.* **46**, L999 (1985).
- [6] H. J. Herrmann, A. Hansen and S. Roux, *Phys. Rev. B* **39**, 637 (1989).
- [7] B. Skjetne, T. Helle and A. Hansen, *To be published*.
- [8] P. L. Larsson, *Compos. Struct.* **11**, 121 (1989).
- [9] B. R. Seshadri and J. C. Newman Jr., "Analyses of Buckling and Stable Tearing in Thin-Sheet Materials", Technical Memorandum NASA-TM-1998-208428, Langley Research Center, Hampton, Virginia (1998).
- [10] W. Li and T. Siegmund, *Eng. Fract. Mech.* **69**, 2073 (2002).
- [11] M. Deng and C. T. J. Dodson, *Paper - An Engineered Stochastic Structure*, (TAPPI Press, Atlanta, 1994).
- [12] Y. B. Seo, R. C. de Oliveira and R. E. Mark, *J. Pulp Pap. Sci.* **18**, 55 (1992).
- [13] B. P. Cherepanov, *J. Appl. Math. Mech.* **27**, 405 (1963).
- [14] M. S. Dyshel, *Sov. Appl. Mech.* **14**, 1169 (1978); **18**, 924 (1982); A. N. Guz, G. G. Kuliev and I. A. Tsurpal, *Eng. Fract. Mech.* **10**, 401 (1978); Y. M. Dal, *Sov. Appl. Mech.* **17**, 693 (1981); H. P. Rossmann, H. Troger and E. Tschegg, *Z. Flugwiss. Weltraum.* **5**, 36 (1981); T. Fujimoto and S. Sumi, *JSME. Int. J.* **30**, 1714 (1987).
- [15] K. Markström and B. Storåkers, *Int. J. Solids Struct.* **16**, 217 (1980);
- [16] G. C. Sih and Y. H. Lee, *Theor. Appl. Fract. Mec.* **6**, 129 (1986);
- [17] D. Shaw and Y. H. Huang, *Eng. Fract. Mech.* **35**, 1019 (1990).
- [18] R. G. Forman, "Experimental Program to Determine Effect of Crack Buckling and Specimen Dimensions on Fracture Toughness of Thin Sheet Materials", Technical Report AFFDL-TR-65-146, Air Force Flight Dynamics Laboratory, Dayton, Ohio (1966).
- [19] J. R. Dixon and J. S. Strannigan, "Stress Distributions and Buckling in Thin Sheets with Central Slits", in *Proc. Second Int. Conf. on Fracture*, pp. 105-118, edited by P. L. Pratt *et al.*, (Chapman and Hall, 1969).
- [20] G. F. Zielsdorff and R. L. Carlson, *Eng. Fract. Mech.* **4**, 939 (1972).
- [21] M. Petyt, *J. Sound Vib.* **8**, 377 (1968).
- [22] E. Riks, C. C. Rankin and F. A. Brogan, *Eng. Fract. Mech.* **43**, 529 (1992).
- [23] A. Barut, E. Madenci, V. O. Britt and J. H. Starnes Jr., *Eng. Fract. Mech.* **58**, 233 (1997).
- [24] A. N. Guz and M. S. Dyshel, *Theor. Appl. Fract. Mec.* **41**, 95 (2004).

- [25] A. N. Guz and M. S. Dyshel, *Theor. Appl. Fract. Mec.* **38**, 103 (2002); M. S. Dyshel, *Mech. Compos. Mater.* **38**, 435 (2002).
- [26] R. L. Carlson and D. F. Riggs, *Israel J. Technol.* **14**, 159 (1976).
- [27] A. N. Guz and M. S. Dyshel, *Theor. Appl. Fract. Mec.* **36**, 57 (2001).
- [28] M. S. Dyshel, *Int. Appl. Mech.* **38**, 472 (2002).
- [29] M. S. Dyshel, *Int. Appl. Mech.* **39**, 1081 (2003).
- [30] D. A. Pellett, R. G. Costello and J. E. Brock, *AIAA. J.* **6**, 2012 (1968).
- [31] A. Gilabert, P. Sibillot, D. Sornette, C. Vanneste, D. Maugis and F. Muttin, *Eur. J. Mech. A-Solid.* **11**, 65 (1992).
- [32] S. Shimizu and S. Yoshida, *Thin Wall. Struct.* **12**, 35 (1991).
- [33] M. R. Hestenes and E. Stiefel, *Nat. Bur. Stand. J. Res.* **49**, 409 (1952).
- [34] R. J. Roark and W. C. Young, *Formulas for Stress and Strain*, (McGraw-Hill Book Company, New York, 1975).
- [35] A. Hansen, E. L. Hinrichsen and S. Roux, *Phys. Rev. B* **43**, 665 (1991).
- [36] B. Skjetne, T. Helle and A. Hansen, *To be published*.